Calibration of the Local Magnitude Scale (M_L) for Eastern Cuba

Eduardo R. Diez Zaldivar[1] , Denis Sandron[*2] , and Manuel Cutie Mustelier[1]

Abstract

Calibration of the local magnitude scale to match local tectonics is a key element in the development of research leading to seismic risk assessment and quantification of seismicity in active regions. In this study, we developed a local magnitude scale for the southeastern region of Cuba—the part of the island exposed to the greatest seismic hazard due to its proximity to the Oriente fault system. From the 2011–2021 Cuban catalog, 7750 earthquakes with $M_\mathrm{L} > 2$ were selected, distributed in the region 19°–22° N, 73°–79° W, and recorded by at least four seismic stations (of the Cuban CW network) within 500 km of the hypocentre. The resulting input data set includes 33,916 amplitude measurements of the horizontal components. We set up the whole linear regression analysis procedure in the Matlab environment to obtain the formula for the local magnitude in the International Association of Seismology and Physics of the Earth's Interior form. In a three-step procedure, we (1) removed the outliers; (2) searched for the parameters n, K, and Si that minimize the unbiased sample standard deviation of the residuals; and (3) set the anchor point for the parameter C. Thus, the new formula for the local magnitude M_L is defined as follows: $M_\mathrm{L} = \log_{10}(A) + 1.000\log_{10}(R) + 0.003R - 1.963$, in which A is the peak amplitude in nanometers simulated with a Wood–Anderson sensor, and R is the hypocentral distance in kilometers. We also calculated the station correction factors S for each station included in the analysis.

Introduction

The local magnitude (M_L) of an earthquake was defined by Richter (1935) as the logarithm of the maximum amplitude from zero to the maximum peak measured on a Wood-Anderson (WA) instrument with 2800 amplification and a natural period of 0.8 s (Anderson and Wood, 1925).

The scale allows the evaluation of earthquake energy and was the first attempt to create an international standard for quantifying the basic parameters of the earthquake. It was defined as follows:

$$M_\mathrm{L} = \log_{10} A(R) - \log_{10} A_0(R), \qquad (1)$$

in which $\log_{10} A(R)$ is the logarithm of the zero-to-peak amplitude in mm in a WA seismogram; R is the epicentral distance in km, and $-\log_{10} A_0(R)$ is the distance correction. The "calibration point" was determined by setting $M_\mathrm{L} = 0$ for a displacement amplitude of 1 thousandth of a millimeter at 100 km of epicentral distance. Thus, the original Richter attenuation curve $(-\log_{10} A_0(R))$ at 100 km is equal to 3. Richter estimated the value of $-\log_{10} A_0(R)$ for distances up to 600 km, taking into account local conditions in southern California.

However, Richter's formula can be adjusted to determine the magnitude in a given area and reduce regional effects on wave propagation.

More recently, a hundredth of a millimeter at 17 km was chosen as an alternative anchor point in the calibration performed for southern California (Hutton and Boore, 1987).

Later, Uhrhammer and Collins (1990) established a new value for the static gain of 2080, found that the value of 2800 corresponding to the static amplification of the WA instrument was incorrect, and resulted in an M_L overestimation. This value was also recently confirmed using data from an original WA instrument still in use (Sandron *et al.*, 2015).

In 2013, the International Association of Seismology and Physics of the Earth's Interior (IASPEI; International Association of Seismology and Physics of the Earth's Interior [IASPEI], 2013) Magnitude Working Group proposed the following general equation:

1. Centro Nacional de Investigaciones Sismológicas (CENAIS), Santiago de Cuba, Cuba, https://orcid.org/0000-0002-1323-8451 (ERDZ); https://orcid.org/0000-0001-7909-8925 (MCM); 2. Istituto Nazionale di Oceanografia e di Geofisica Sperimentale—OGS, Sgonico, Italy, https://orcid.org/0000-0002-1143-9954 (DS)

*Corresponding author: dsandron@ogs.it

$$M_L = \log_{10}(A) - n\log_{10}(R) - KR - C - S, \qquad (2)$$

in which A is the maximum amplitude in nanometers recorded by a simulated instrument such as WA with a static gain of 1; R is the hypocentral distance in kilometers; C is a constant; and S is the correction per station due to local conditions (Bormann and Dewey, 2012). The parameters n and K represent geometrical spreading and anelastic attenuation, respectively (Bakun and Joyner, 1984).

However, the M_L estimate can be affected by local amplitude variations that depend on the station location due to the source radiation pattern, local noise, and crustal structure (Havskov and Ottemoller, 2010). Therefore, it is advisable to perform the calibration of equation (2) for the specific conditions and tectonic environment of each geographic region.

In general, the IASPEI recommends the use of the following equation for regions that do not yet have a local magnitude law with the appropriate parameters and that have attenuation characteristics similar to southern California:

$$M_L = \log_{10}(A) + 1.11\log_{10}(R) + 0.00189R - 2.09. \qquad (3)$$

This equation is quite similar to that proposed by Hutton and Boore (1987) and is consistent with Ritcher's M_L equation.

Several studies have been conducted to calibrate the M_L equation coefficients for different geographical areas around the world, for example, for Europe, the results can be found in Bragato and Tento (2005), Bobbio *et al.* (2009), DiBona (2016) for Italy; Scordilis *et al.* (2013) for Greece; Chovanová and Kristek (2018) for Slovakia; Ottemoller and Sargeant (2013) for the United Kingdom; and Baumbach *et al.* (2005) for Turkey and others. Keir *et al.* (2006), Brazier *et al.* (2008), and Shumba *et al.* (2023) have obtained the coefficients of the general equation proposed by IASPEI for different regions of Africa, whereas contributions have been published by Kim and Park (2005) for the Korean peninsula in Asia and Oceania; Vishwa *et al.* (2020) for a region of India; and Rhoades *et al.* (2021) for New Zealand. In the Americas, the research of Condori *et al.* (2017) for Peru; Rengifo and Ojeda (2004) for Colombia; and the results of Hutton and Boore (1987) and Miao and Langston (2007).

In Cuba, in particular, since the establishment of seismological stations in 1964, different approaches have been used to determine the local magnitudes of earthquakes. Álvarez and Bune (1977) and Álvarez *et al.* (1999, 2000) estimated the parameters for magnitude calculation using the results obtained for the evaluation of the energy class K or K-class, which is an earthquake force or magnitude measure of local and regional earthquakes used in countries of the former Soviet Union, Cuba, and Mongolia, Rautian *et al.* (2007).

The first equation of M_L, equivalent to the Richter magnitude scale for the Cuban territory, was proposed by Moreno and González (2001) and was based on the analysis of

earthquake records using data from the old short-period stations installed at that time, which was quite limited in terms of quantity and quality.
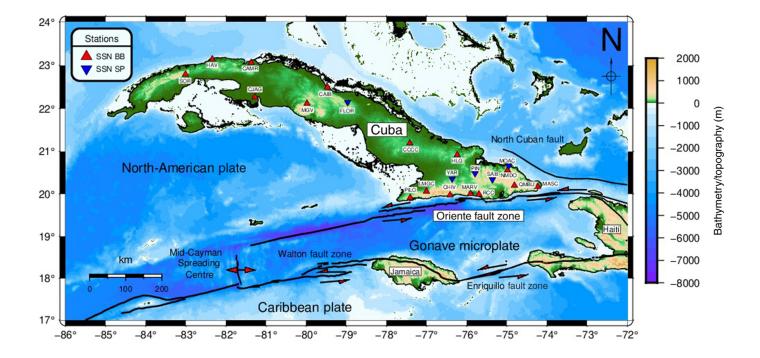
Later, the seismic network was upgraded and converted to digital, with the installation of broadband stations, which increased the station's density in southeastern Cuba and allowed the calculation from digital records. With the new database, Moreno (2002) updated the parameters of the M_L, considering a new data set. This equation is currently used by the Centro Nacional de Investigaciones Sismológicas (CENAIS). However, in the last 20 yr, new stations have been deployed in the same study region, using new instruments with higher gain and wider frequency response and dynamic range (Diez Zaldívar *et al.*, 2014). To this day, Cuba has not seen the development of a comprehensive method for estimating M_L equation parameters using a large number of seismic stations and many years of recorded data.

This situation motivated the need to conduct a study to recalibrate the parameters of the M_L equation with the highest precision and focusing on the southeastern part of Cuba.

The Tectonic Environment in the Study Area

Geographically, the island of Cuba belongs to the Caribbean—the area in the west of the northern Atlantic Ocean between North and South America. From a geological and tectonic point of view, it is a complex region for which different and sometimes controversial views on its evolution have been formulated over time. Figure 1 shows the location of Cuba in the tectonic context of the Caribbean. Initially, some authors claimed that Cuba belongs to the North American tectonic plate, and that its southeastern margin is adjacent to the Caribbean plate (Mann *et al.*, 1995; Lundgren and Russo, 1996; Mann, 1999). This margin approaches a transcurrent fault system parallel to the coast and exhibits left-lateral motion known as the "Oriente" fault system zone (also called the "Bartlett-Caymán" zone; Calais and Lépinay, 1993). This tectonic structure affects not only the territory of Cuba but also other Caribbean islands such as Jamaica, the Cayman Islands, Puerto Rico, and Hispaniola. However, some recent studies on this plate boundary zone (Calais and Lépinay, 1989, 1993; DeMets, 1990; Deng and Sykes, 1995), also based on arguments based on crustal deformation modeling, have demonstrated the existence of a microplate between the North American and Caribbean plates, namely the Gonave microplate, previously proposed by Rosencrantz and Mann (1991) (Fig. 1).

The Gonave microplate is a semirectangular microplate with an area of about 190,000 km^2 that borders the North American plate to the south and the Caribbean plate to the north (Heubeck and Mann, 1991; Mann *et al.*, 2004). The "Oriente" fault zone is responsible for most of the strong earthquakes in this area, as inferred from estimates of the energy accumulated by the relative motion between the plates described earlier (Arango, 2009).

Figure 1. The Cuba island in the Caribbean tectonic context. The main fault systems (black lines; red arrows represent the fault relative movement) with the Bartlett–Cayman fault system (Oriente) and other relevant fault systems in the region (Mann *et al.*, 1995, 2004; Lundgren and Russo, 1996; Mann, 1999). In addition, the maps represent the stations of the Cuban seismic network, the red triangles correspond to the broadband stations, and the inverted blue triangles show the short-period seismic stations. The color version of this figure is available only in the electronic edition.

Seismicity

This study covered a geographical area between 19°–22° N and 73°–79° W. In this area, the predominant seismicity is characterized by an "interplate" behavior related to the Oriente fault zone, and presents a higher frequency of earthquakes that can reach a large magnitude ($M_w > 6.0$) and a depth greater than 20 km. More than 90% of the earthquakes that strike the country occur in this southeastern area of Cuba (Álvarez and Menendez, 1969; Álvarez and Bune, 1977; Moreno *et al.*, 2002). However, moderate seismicity has also been associated with minor faults in the interior of Cuba that have produced some moderate earthquakes with significant damage (Chuy, 1999).

The map in Figure 2 shows earthquakes recorded in Cuba since 2011 and until 2021 (or events with a magnitude between 2 and 5 we used the M_L scale, whereas for earthquakes exceeding this value, we considered the M_w magnitude), showing the prevalence of interplate seismicity. Historical earthquakes, which are not shown on this map, follow the same trend in terms of location and intensity (Chuy, 1999).

In addition to the large and moderate earthquakes, it is also important to accurately record the weak seismicity, because it is crucial for defining the seismic regime of the whole area, as well as for estimating the accumulation or release of tectonic deformation, the dispersion and attenuation properties of the crust, and seismic hazard (Arango, 2021). The map in Figure 1a of this document shows all earthquakes recorded between the years 2011 and 2021.

Cuban Seismic Network

Two periods can be distinguished in the operation of the Cuban seismic network: the first, from the mid-1960s to 1997, with main stations equipped with short-period analog instruments and photographic–visual records (Serrano and Álvarez, 1983); and the second, from 1998 to the present day, characterized by digital instruments, either short-period, broadband or accelerometers (Diez Zaldívar *et al.*, 2014). Currently, the Cuban seismic network consists of 21 stations distributed throughout the island, transmitting data in real-time to the CENAIS geodynamic observatory in Santiago de Cuba. In the study area, traces from 14 stations (10 broadband and 4 short-period) were used to calibrate the M_L scale. In addition, traces from GBTY station (Guantanamo Bay Naval Base, CU network) were included. This station is not part of the Cuban network but is geographically located in Cuban territory, which was included (see Table 1). The map in Figure 2 shows the geographic location of the stations (see legend). The technical specifications of the Cuban seismic network and its performance in terms of noise, as well as the evaluation of event detection rates, can be found in Diez Zaldivar *et al.* (2022).

Data Selection

Between 2011 and 2021, the Cuban seismic network recorded more than 60,000 earthquakes with fairly well-determined
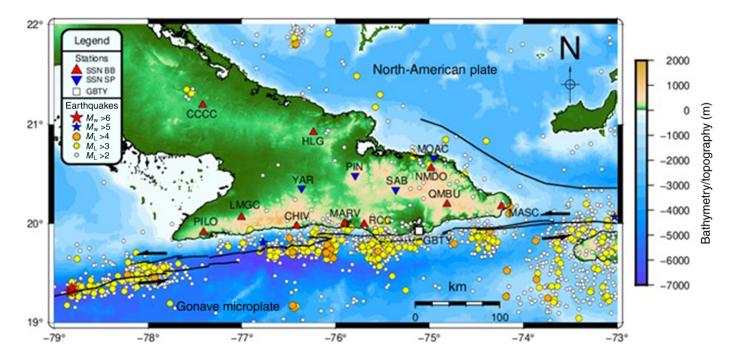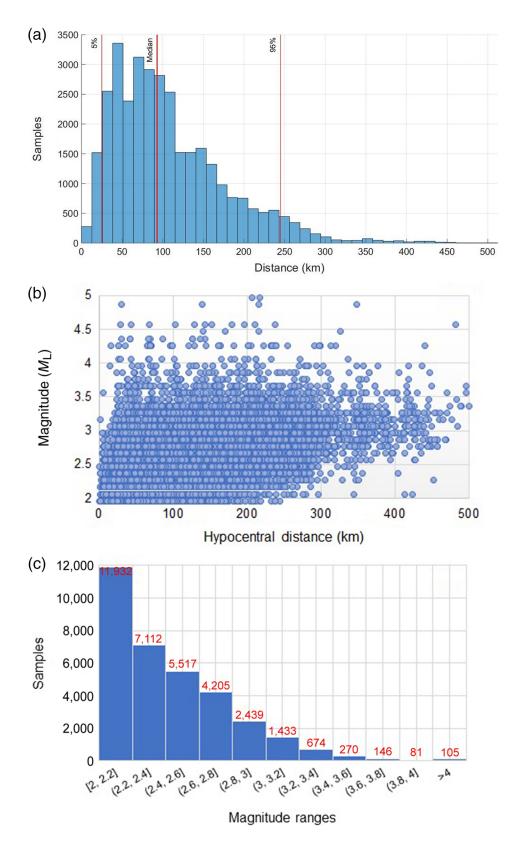
Figure 2. Seismicity in Cuba and surrounding areas from 2011 to 2021, taken from the CENAIS historical general catalog and reprocessed for this study by authors. The magnitude ranges from 2 to 7 or more is considered (see colors in the legend). The red tri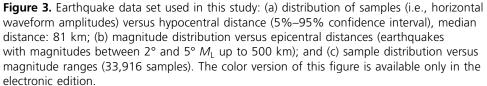angles represent the broadband stations, and the inverted blue triangles show the short-period stations of the Cuban network. The Oriente fault is explicitly shown (black line). We used local magnitude M_L for magnitude not exceeding 5 and moment magnitude M_w for stronger events. The color version of this figure is available only in the electronic edition.

TABLE 1
Details of the Stations of the Cuban Seismic Network and GTBY

Station Name	Network Code	Station Code	Latitude (°N)	Longitude (°W)	Instruments
Chivirico	CW	CHIV	19.9764	76.4151	Trillium Compact 120s (Centaur)
Cascorro	CW	CCCC	21.1934	77.4173	Trillium 120P (Centaur)
Holguín	CW	HLG	20.9200	76.2361	Trillium 120P (Centaur)
Las Mercedes	CW	LMGC	20.0646	77.0045	BBVS-60s (EDAS-24IP)
Nuevo Mundo	CW	NMDO	20.5598	77.4173	Trillium 120P (Centaur)
Mar Verde	CW	MARV	20.0052	75.9065	Trillium Compact 120s (Centaur)
Maisí	CW	MASC	20.1755	74.2312	CME-6211 60s (Baykal 8)
Pilón	CW	PILO	19.9140	77.4085	CME-6211 60s (Baykal 8)
Pinares Mayarí	CW	PIN	20.4855	75.7915	FSS-3M 2s (EDAS-24IP)
Quimbuelo	CW	QMBU	20.1989	74.8127	Trillium Compact 120s (Centaur)
Rio Carpintero	CW	RCC	19.9950	75.6965	Trillium 120P (Centaur)
Sabaneta	CW	SAB	20.3418	75.3593	FSS-3M 2s (EDAS-24IP)
Yarey	CW	YAR	20.3577	76.3635	FSS-3M 2s (EDAS-24IP)
Moa	CW	MOAC	20.6654	74.9550	FSS-3M 2s (EDAS-24IP)
Guantanamo Bay	CU	GTBY	19.9268	75.1108	Standard gain STS-2 (Quanterra)

Seismic network stations characteristics (only those used in this study).

Figure 3. Earthquake data set used in this study: (a) distribution of samples (i.e., horizontal waveform amplitudes) versus hypocentral distance (5%–95% confidence interval), median distance: 81 km; (b) magnitude distribution versus epicentral distances (earthquakes with magnitudes between 2° and 5° M_L up to 500 km); and (c) sample distribution versus magnitude ranges (33,916 samples). The color version of this figure is available only in the electronic edition.

parameters. These earthquakes were analyzed by CENAIS seismologists, and different signal processing methods were applied such as filtering, deconvolution with the instrument transfer function, and simulation of the WA seismometer by SEISAN software (Havskov and Ottemoller, 2000).

Data were obtained from the Cuban Seismological Service general catalog—CENAIS (2023). Our selection criteria were: M_L in a range between 2 and 5, to avoid the saturation phenomenon of the M_L scale (Bormann, 2002); and a minimum of four triggering stations. The selection includes 7750 seismic events, and the final input data set includes a total of 33,916 records that include: the event ID, dates, depth, horizontal component amplitudes, calculated epicentral hypocentral distance, and the number of stations detected for each seismic event. This data set is provided as part of this study in the supplemental material available to this article.

Figure 3 illustrates some features of the data set: Figure 3a shows the distribution of samples as a function of hypocentral distance; Figure 3b shows earthquake distribution with distance (up to 500 km), emphasizing that most events are located at a distance of less than 300 km; and Figure 3c shows the distribution of samples versus distance as a function of M_L value.

From these figures, we can conclude that the study area is covered well enough, both in terms of magnitude and distance, to apply the inversion method.

Figure 4. Residuals distribution: (a) results of the first iteration for the removal procedure using the initial data set, the red circles show the residual values considered as outliers, and the red lines represent the limits used to define the outliers; (b) the first step of removal (number of samples versus residual values); (c) last iteration results without outliers (33,325 samples); and (d) last step of removal (number of samples versus residual values). The color version of this figure is available only in the electronic edition.

Method

Following Chovanová and Kristek (2018), we assume that N_e is the number of events (7750), and N_s is the number of stations records for which were analyzed; we can reformulate an over-determined system of equations from equation (2) as follows:

$$\log_{10}(A_{ji}) = M_{L_j} + n \log_{10}(R_{ji}) + K R_{ji} + S_i + C, \quad (4)$$

in which $j = 1, \ldots, N_e$ is the jth event; and $i = 1, \ldots, N_s$ represents the ith seismic station.

Because the local magnitude of the jth event (M_{L_j}) and the constant C are coupled, we can define M_j as follows:

$$M_j = M_{L_j} + C. \quad (5)$$

Thus, equation (4) becomes as follows:

$$\log_{10}(A_{ji}) = M_j + n \log_{10}(R_{ji}) + K R_{ji} + S_i. \quad (6)$$

More details can be found in Chovanová and Kristek (2018).

Results and Discussions

In the first step of our procedure, we remove the outliers from the data set by solving equation (6) for n, K, and S_i and evaluating the residuals r_{ji} as follows:

$$r_{ji} = \log_{10}(A_{ji}) - (M_j + n \log_{10}(R_{ji}) + K R_{ji} + S_i). \quad (7)$$

The goal is to obtain a data set from which these values have been removed. To do this, we defined outliers as values of r_{ji}

that fall outside 1.5 times the interquartile range of residuals, and then we solved equation (7) repeatedly, and starting from the original data set (33,829 records), after five iterations, 1.5% of the data (504 records) were considered outliers and consequently removed.

Figure 4a shows the values of r_{ji} as a function of distance after the first removal step according to the previously defined bounds, with the values outside the defined bounds indicated by red circles, and Figure 4b shows the distribution of the samples versus the residuals determined for this first step. Figure 4c,d shows the same results for the last step.

The second step involved the estimation of the n, K, and S_i parameters in such a way that the standard deviation σ is minimized,

$$\sigma = \sqrt{\frac{\sum r_{ji}^2}{N - (N_e + N_s + 1)}}, \quad (8)$$

in which N_e is the number of estimated magnitudes M_j; and N_s is the number of estimated corrections per station S_i. For the calculation of this parameter, a grid search was used, consisting
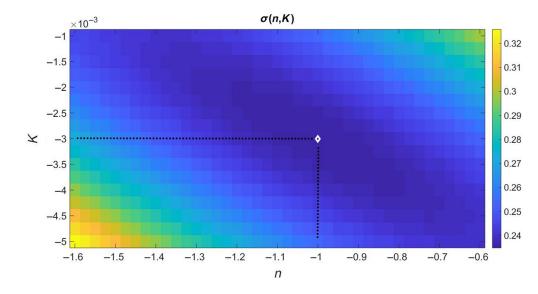
Figure 5. The unbiased sample standard deviation (σ) of residuals as a function of parameters n and K. The white diamond indicates the minimum deviation. The color version of this figure is available only in the electronic edition.
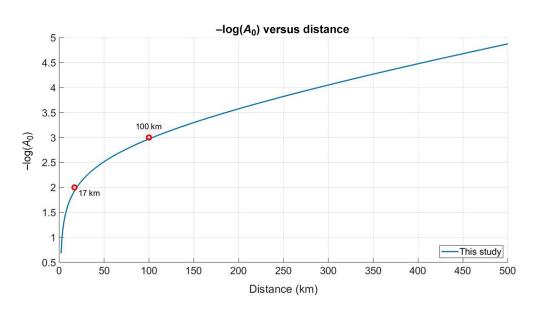

Figure 6. The attenuation curve computed in this study for southeastern Cuba (up to 500 km). The red circles indicate the anchor points proposed by Richter (1935) and Hutton and Boore (1987). The color version of this figure is available only in the electronic edition.

inserting S_i as an unknown, one can separate the systematic errors at each station from the residuals.

Figure 5 shows the values of the standard deviation σ as a function of the parameters n and K. The white diamond points to the minimum value of σ. This corresponds to the values of $n = -1.000$ and $K = -0.003$.

Both the parameters have negative values, which is consistent with the fact that both are related to attenuation. The higher the geometric scattering term, the lower the damping of the anelastic scattering, and vice versa.

The following step regards the definition of the C constant, according to Richter's magnitude definition:

$$C = M - \log_{10}(A) + n\log_{10}(R) + KR, \qquad (10)$$

and the station correction parameters S_i, which has to satisfy the condition that their sum is zero:

$$\sum_{i=1}^{N_s} S_i = 0. \qquad (11)$$

Because of the variation in attenuation values within the first 100 km, we chose an anchor point (1/100th millimeter at 17 km) following Hutton and Boore (1987).

We applied equation (10) with values $n = -1.000$ and $K = -0.003$, and obtained the value of

$$C = -1.963.$$

The final equation obtained for M_L in our study is as follows:

$$M_{Lj} = \log_{10}(A_{ji}) + 1.000\log_{10}(R_{ji}) + 0.003R_{ji} - 1.963, \qquad (12)$$

in which j is the jth event, and i is the ith seismic station.

of 972 points, in which an interval for n was set in the range between -0.6 and -1.6 with a step of 0.025, and for the parameter K an interval between -0.0050 and -0.0010 with a step of 0.00025.

Rewriting equation (6), we obtain the following equation:

$$\log_{10}(A_{ji}) - n\log_{10}(R_{ji}) - KR_{ji} = M_j + S_i. \qquad (9)$$

For each n and K in the interval, one obtains the values of M_j and S_i, and then, using equation (8), the value of σ. By

TABLE 2
Magnitude Correction for Each Station and Type of Soil

Network Code	Station Code	Latitude (° N)	Longitude (° W)	Station Correction	Type of Soil
CW	CHIV	19.976	76.415	−0.041	Volcanic ash-forming layers or strata
CW	CCCC	21.193	77.417	0.264	Very-hard igneous rocks (granite)
CW	HLG	20.920	76.236	−0.081	Igneous rocks (streamers)
CW	LMGC	20.064	77.004	−0.389	Volcanic ash-forming extracts
CW	NMDO	20.559	77.417	0.158	Igneous rocks (streamers)
CW	MARV	20.005	75.906	0.050	Igneous rocks (basalts)
CW	MASC	20.175	74.231	0.237	Sedimentary rock (hard limestones)
CW	MOAC	20.665	74.955	0.137	Ophiolites rocks
CW	PILO	19.914	77.408	−0.308	Stratified volcanic rocks
CW	PIN	20.485	75.791	−0.336	Streamers
CW	QMBU	20.198	74.812	−0.168	Compact clusters
CW	RCC	19.995	75.696	0.221	Very-hard igneous rocks
CW	SAB	20.341	75.359	−0.083	Stratified limestones
CW	YAR	20.357	76.363	0.370	Basalt rocks
CU	GTBY	19.926	75.110	−0.033	Sediments

Figure 6 shows the attenuation curve $-\log_{10}(A_0)$ as a function of distance using the parameters determined in this study for the southeastern region of Cuba for distances up to 500 km. The red circles show the anchor points proposed by Richter and Hutton and Boore.

Finally, we calculated the correction parameter S_i for each station; the results are shown in Table 2 and Figure 7.

For the station correction S_i, we determined the values for the 15 seismic stations used in this study (Table 2). The values of the station corrections range up to ±0.30. The determined parameters are generally consistent with the local geology, that is, large negative corrections for stations on unconsolidated rocks (GBTY, LMGC, and PILO) and positive corrections for stations on hard rocks (CCCC, RCC, and YAR). Other stations located on certain rock types have correction values close to zero; it should be noted that these corrections are related to the network used and are, on average, zero.

In the southeastern part of Cuba, specifically the Oriente fault, the most significant local structures affecting the tectonic regime are the Cabo Cruz basin and the Santiago deformed belt. These structures are responsible for 85%–90% of the recorded seismicity. According to Calais and Mercier de Lépinay (1991), the Cabo Cruz basin is an east–west-trending depression bounded to the north and south by the Oriente fault, and divided by a series of normal faults (series of oblique faults that generate local stresses).

The Santiago deformed belt is a narrow mountain range that extends along the Oriente fault in the eastern half of the south coast of the island; its main characteristics and description of its morphology can be found in Calais and Mercier de Lépinay (1990). This complex crustal structure causes widely dispersed seismic waves along the plate boundary. In addition, the seismicity in Cuba is clustered in a few seismogenic sources (Moreno, 2002), which means that the distribution of earthquakes is not homogeneous throughout the study area; the attenuation along the path should be considered as a possible factor affecting the station correction.

These characteristics together with the local geological conditions are responsible for the divergence in the station correction parameter S_i values.

The newly developed M_L scale for southeastern Cuba shows that the coefficients n and K are quite similar to those obtained by other authors, and the attenuation curve obtained lies between those of Hutton and Boore (1987) and Moreno (2002), without significant changes (Fig. 8a). However, for short distances, small differences are obtained, not exceeding 5% (Fig. 8b). Looking at the curve previously calibrated for Cuba, the difference in size calculation as a function of hypocentral distance (Fig. 8c) between this study is maintained at ΔM_L values of 0.04, starting with a negative curve of −0.04, an intercept at 30 km, and culminating in a positive curve (0.04) up to 100 km.
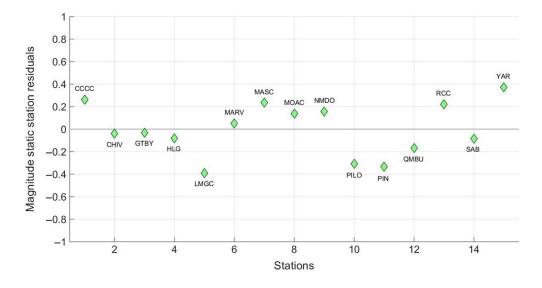
Figure 7. Values of the station correction parameter S_i in the final magnitude formula (green diamonds) for stations used in this study. The color version of this figure is available only in the electronic edition.

Conclusions

In our study, we determined the values of the coefficients of the M_L equation based on Ritcher's original definition and chose 17 km as the anchor point according to Hutton and Boore (1987). The local attenuation curve or distance correction for southeastern Cuba was estimated by linear regression analysis procedure using the measured horizontal components amplitudes (33,916) in the traces of 7750 earthquakes with $M_L > 2$ from the 2011–2021 CENAIS catalog, distributed in the region 19°–22° N; 73°–79° W and recorded by at least four seismic stations of the Cuban (CW) network and the GBTY (CU) station, within 500 km of the hypocentre.

This calculation provided values for the empirical coefficients for geometrical spreading and anelastic attenuation that control the amplitude–distance correction curve.

The curve found is slightly less attenuated than that previously defined for this area by Moreno (2002) and lies in between that and the curve obtained for California by Hutton and Boore (1987).

The correction values found for the stations are consistent with the local geology.

We can conclude that the M_L scale, proposed in this study, can replace the local magnitude scale, currently used in the routine work of CENAIS.

Data and Resources

The Cuban seismic network (Servicio Sismologico Nacional [SSN]) available at www.cenais.cu (last accessed August 2023—Rev. Fac. Ing. UCV, June 2014, Vol. 29, no. 2, pp. 69–77. ISSN 0798-4065) is managed by the Centro Nacional de Investigaciones Sismologicas (CENAIS) of the Ministerio de Ciencia, Tecnologia y Medio Ambiente (CITMA). The general SSN earthquake catalog is available for consultation at http://www.cenais.cu (last accessed July 2023). All stations are registered at the International Federation of Digital Seismograph Networks (FDSN) available at http://www.fdsn.org/ (last accessed August 2023). The following software systems were used: SEISAN (Havskov and Ottemoller, 2000) available at https://www.uib.no/en/rg/geophysics/54592/software#seisan (last accessed August 2023); Generic Mapping Tools (GMT; Wessel and Smith, 1991; Wessel et al., 2013; Generic Mapping Tools [GMT], 2023) available at https://www.generic-mapping-tools.org (last accessed August 2023); AWK (Aho et al., 1987), with its GNU implementation: GAWK available at www.gnu.org/software/gawk (last accessed August 2023); and MATLAB, version 9.0.0 (R2019b), Natick, Massachusetts, U.S.A.: The MathWorks Inc. available at https://www.mathworks.com/products/matlab.html (last accessed August 2023). This article is accompanied by the supplemental material, which includes the earthquake catalog from 2011 to 2021 recorded by the Cuban SSN (catalog_2011_2021.out).
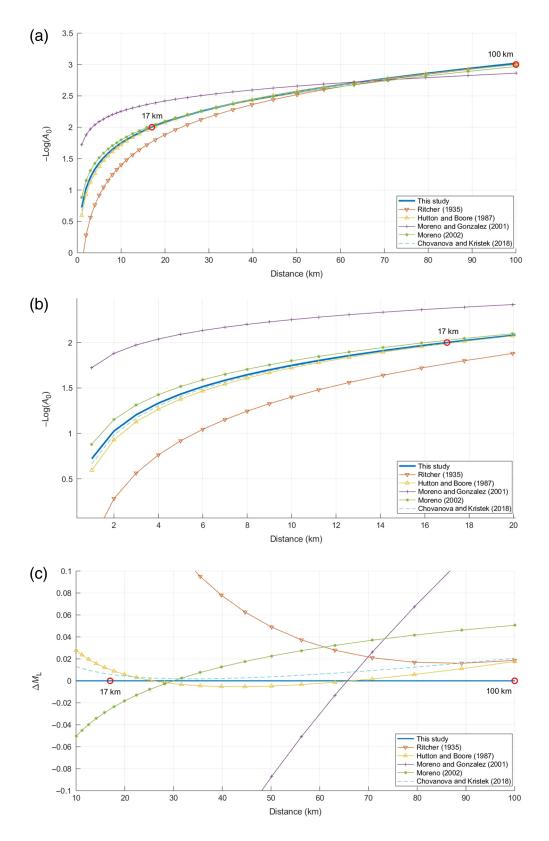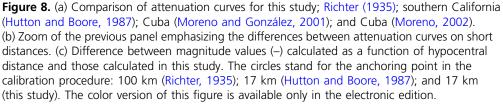
Declaration of Competing Interests

The authors acknowledge that there are no conflicts of interest recorded.

Acknowledgments

Figure 8. (a) Comparison of attenuation curves for this study; Richter (1935); southern California (Hutton and Boore, 1987); Cuba (Moreno and González, 2001); and Cuba (Moreno, 2002). (b) Zoom of the previous panel emphasizing the differences between attenuation curves on short distances. (c) Difference between magnitude values (–) calculated as a function of hypocentral distance and those calculated in this study. The circles stand for the anchoring point in the calibration procedure: 100 km (Richter, 1935); 17 km (Hutton and Boore, 1987); and 17 km (this study). The color version of this figure is available only in the electronic edition.

References

Aho, A. V., B. W. Kernighan, and P. J. Weinberger (1987). *The AWK Programming Language*, Addison-Wesley Longman Publishing Co., Inc., Boston, Massachusetts, U.S.A.

Álvarez, H., and A. Menendez (1969). Sismicidad de Cuba, *Izv. Akad. Naukk S.S.S.R. Fizika Zemli* **1,** 74–78 (in Russian).

Álvarez, J. L., and V. I. Bune (1977). Seismic hazard assessment for southeastern Cuba, *Izv. Akad. Naukk S.S.S.R. Fizika Zemli* **10,** 54–67 (in Russian).

Álvarez, L., T. Chuy, J. García, B. Moreno, H. Álvarez, M. Blanco, O. Expósito, O. González, and A. I. Fernández (1999). An earthquake catalogue of Cuba and neighbouring areas, *ICTP Internal Rept. ic/ir/99/1*, Miramare, Trieste, Italy, 60, available at http://iohanis.com/~leoalvar/papers/ICTPcata.pdf (last accessed November 2023).

Álvarez, L., R. S. Mijailova, E. O. Vorobiova, T. J. Chuy, G. N. Zhakirdzhanova, E. R. Perez, L. M. Rodionova, H. Alvarez, and K. M. Mirzoev (2000). Terremotos de Cuba y áreas aledañas, in *Sismicidad de Cuba y estructura de la corteza en el Caribe*, J. L. Alvarez (Editor) Editorial Academia, La Habana, Cuba, 7–35 (in Spanish).

Anderson, J. A., and H. O. Wood (1925). Description and theory of the torsion seismometer, *Bull. Seismol. Soc. Am.* **15,** no. 1, 1–72, doi: 10.1785/BSSA0150010001.

Arango, E. D. (2009). Análisis geodinámico y sismotectónico del extremo oriental de Cuba, *Acta GGM D.ebrecina* **4,** 43–52 (in Spanish).

Arango, E. D. A. (2021). Sismicidad Registrada en el territorio nacional y estado de la red de estaciones del

servicio sismológico nacional, *Vicedirección Técnica, Archivos de Centro Nacional de Investigaciones Sismológicas, Ministerio de Ciencia, Tecnología y Medio Ambiente, 2020*, available at https://www.cenais.gob.cu/cenais/ (last accessed November 2023) (in Spanish).

Bakun, W. H., and W. B. Joyner (1984). The ML scale in central California, *Bull. Seismol. Soc. Am.* **74,** 1827–1843.

Baumbach, M., D. Bindi, H. Grosser, C. Milkereit, S. Paralai, R. Wang, S. Karakisa, S. Zunbul, and J. Zschau (2005). Calibration of an ML scale in northwestern Turkey from 1999 Izmit aftershocks, *Bull. Seismol. Soc. Am.* **93,** no. 5, 2289–2295, doi: 10.1785/0120020157.

Bobbio, A., M. Vassallo, and G. Festa (2009). A local magnitude scale for southern Italy, *Bull. Seismol. Soc. Am.* **99,** 2461–2470.

Bormann, P. (2002). *New Manual of Seismological Observatory Practice (NMSOP-2)*, Deutsches GeoForschungszentrum GFZ, Potsdam, Germany, 16–50, doi: 10.2312/GFZ.NMSOP-2.

Bormann, P., and J. W. Dewey (2012). *The New IASPEI Standards for Determining Magnitudes from Digital Data and Their Relation to Classical Magnitudes, New Manual of Seismological Observatory Practice 2 (NMSOP-2)*, Deutsches GeoForschungs Zentrum GFZ, Germany, 1–4.

Bragato, P., and A. Tento (2005). Local magnitude in northeastern Italy, *Bull. Seismol. Soc. Am.* **95,** no. 2, 576–591, doi: 10.1785/0120040100.

Brazier, R., Q. Miao, A. Nyblade, A. Ayele, and C. Langston (2008). Local magnitude scale for the Ethiopian plateau, *Bull. Seismol. Soc. Am.* **98,** 2341–2348.

Calais, E., and M. Lépinay (1989). Géométrie et régime tectonique le long d une limite de plaques en coulissage: la frontiére nordCaraïbe de Cuba á Hispaniola Grandes Antilles, Géodynamique, *C R. Acad. Sci.* **308,** 131–135 (in French).

Calais, E., and M. Lépinay (1993). Semiquantitative modeling of strain and kinematics along the Caribbean/North America strike-slip plate boundary zone, *J. Geophys. Res.* **98,** 8293–8308.

Calais, E., and B. Mercier de Lépinay (1990). A natural model of active transpressional tectonics: The en échelon structures of the Oriente deep along the northern Caribbean transcurrent plate boundary (southern Cuban margin), *Rev. Inst. Fr. Pét.* **45,** 147–160.

Calais, E., and B. Mercier de Lépinay (1991). From transtension to transpression along the Southern Caribbean plate boundary of Cuba: Implications for the recent motion of the Caribbean plate, *Tectonophysics* **186,** 329–350.

Centro Nacional de Investigaciones Sismológicas (CENAIS) (2023). Catálogo de terremotos (extracción parcial de los años 2011 al 2021 del catálogo general de terremotos), *Fondos del CENAIS*, available at https://www.cenais.gob.cu/cenais/ (last accessed July 2023) (in Spanish).

Chovanová, Z., and J. Kristek (2018). A local magnitude scale for Slovakia, Central Europe, *Bull. Seismol. Soc. Am.* **108,** 5A, 2756–2763, doi: 10.1785/0120180059.

Chuy, T. (1999). Macrosísmica de Cuba y su aplicación en los estimados de peligrosidad y microzonación Sísmica, Tesis en opción al Grado de Doctor en Ciencias Geofísicas, Fondos del MES y CENAIS, 150 p. (in Spanish).

Condori, C., H. Tavera, G. Marotta, M. Rocha, and G. S. França (2017). Calibration of the local magnitude scale (ML) for Peru, *J. Seismol.* 21**,** 987–999, doi: 10.1007/s10950-017-9647-3.

DeMets, C. (1990). Earthquake slip vectors and estimates of present-day plate motions, *J. Geophys. Res.* **98,** no. B4, 6703–6714.

Deng, J., and L. Sykes (1995). Determination of Euler polo for contemporary relative motion of Caribbean and North American plates using slip vectors of interpolate earthquakes, *Tectonics* **14,** no 1, 39–53.

DiBona, M. (2016). A local magnitude scale for crustal earthquakes in Italy, *Bull. Seismol. Soc. Am.* **106,** 242–258.

Diez Zaldívar, E. R., M. C. Mustelier, C. M. Moracén, R. P. Cláres, V. Poveda Brossard, Z. Yinxing, C. Yang, and W. Fengxia (2014). Modernización de la red sísmica cubana, Instalación, calibración y puesta a punto, *Rev. Fac. Ing. UCV* **29,** 69–78 (in Spanish).

Diez Zaldivar, E. R., E. Priolo, D. Sandron, V. Poveda Brossard, M. Cattaneo, S. Marzorati, and R. Palau Clares (2022). Evaluation of the event detection level of the cuban seismic network, *Seismol. Res. Lett.* **93,** 2048–2062, doi: 10.1785/0220220016.

Generic Mapping Tools (GMT) (2023). The Generic Mapping Tools documentation, *The GMT Team*, available at https://docs.generic-mapping-tools.org/latest/# (last accessed August 2023).

Havskov, J., and L. Ottemoller (2000). SEISAN Earthquake Analysis Software, *Seismol. Res. Lett.* **70,** 532–534, doi: 10.1785/gssrl.70.5.532.

Havskov, J., and L. Ottemoller (2010). *Routine Data Processing in Earthquake Seismology*, Springer, Netherlands, Dordrecht, 347, doi: 10.1007/978-90-481-8697-6.

Heubeck, C., and P. Mann (1991). Geologic evaluation of plate kinematic models for the North American-Caribbean plate boundary zone, *Tectonophysics* **191,** 1–26.

Hutton, L. K., and D. M. Boore (1987). The ML scale in southern California, *Bull. Seismol. Soc. Am.* **77,** 2074–2094, doi: 10.1785/BSSA0770062074.

International Association of Seismology and Physics of the Earth's Interior (IASPEI) (2013). Summary of magnitude working group recommendations on standard procedures for determining earthquake magnitudes from digital data, available at http://download.iaspei.org/commissions/CSOI/Summary_WG_recommendations_20130327.pdf (last accessed April 2023).

Keir, D., G. Stuart, A. Jackson, and A. Ayele (2006). Local earthquake magnitude scale and seismicity rate for the Ethiopian rift, *Bull. Seismol. Soc. Am.* **96,** 2221–2230.

Kim, S. K., and M. A. Park (2005). The local magnitude scale in the Korean peninsula, *Pure Appl. Geophys.* **162,** 875–889.

Lundgren, P. R., and R. M. Russo (1996). Finite element modeling of crustal deformation in the North America-Caribbean plate boundary zone, *J. Geophys. Res.* **101,** no. B5, 11,317–11,327.

Mann, P. (1999). Caribbean sedimentary basins: Classification and tectonic setting, in *Sedimentary Basins of the World, Caribbean Basins*, Mann, P. (Editor), Elsevier, Amsterdam, Netherlands, 3–31.

Mann, P., E. Calais, and V. Huérfano (2004). Earthquake shakes big bend region of North America Caribbean boundary zone, *Eos Trans. AGU* **85,** 24.

Mann, P., F. Taylor, R. Edwards, and T.-L. Ku (1995). Actively evolving microplate formation by oblique collision and side-ways motion along strike-slip faults: An example from the northeastern Caribbean plate margin, *Tectonophysics* **246,** 1–69.

Miao, Q., and C. A. Langston (2007). Empirical distance attenuation and the local magnitude scale for the central US. *Bull. Seismol. Soc. Am.* **97,** no. 6, 2137–2151, doi: 10.1785/0120060188.
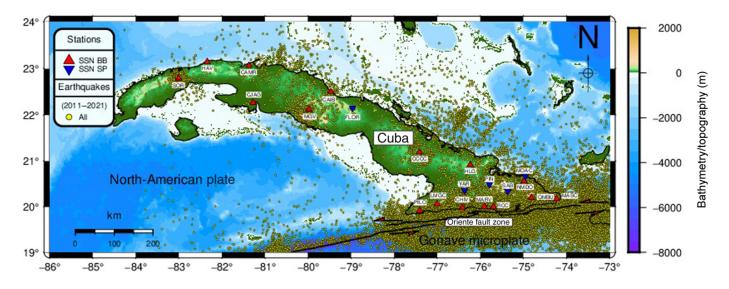
Moreno, B. (2002). New magnitude scales and attenuation relation for eastern Cuba, *Ph.D. Thesis, Crustal Structure and Seismicity of Cuba and Web-Based Applications for Earthquake Analysis,* University of Bergen, Norway.
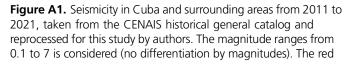
Moreno, B., and O. González (2001). Local magnitude scale for the eastern region of Cuba, in *Sismicidad de Cuba y estructura de la corteza,* J. L. Alvarez Gómez (Editor), Editorial Academia, La Habana, Cuba, ISBN: 978-959-02-0242-1 (in Spanish).

Moreno, B., M. Grandison, and K. Atakan (2002). Crustal velocity model along the southern Cuba margin. Implications for the tectonic regime at an active plate boundary. *Geophys. J. Int.* **151,** 632–645.

Ottemoller, L., and S. Sargeant (2013). A local magnitude scale ml for the United Kingdom, *Bull. Seismol. Soc. Am.* **103,** 2884–2893.

Rautian, T. G., V. I. Khalturin, K. Fujita, K. G. Mackey, and A. D. Kendall (2007). Origins and methodology of the Russian energy K-Class system and its relationship to magnitude scales, *Seismol. Res. Lett.* **78,** no. 6, 579–590, doi: 10.1785/gssrl.78.6.579.

Rengifo, F., and A. Ojeda (2004). Inversión de amplitudes de registros sísmicos para el cálculo de magnitud Ml en Colombia, *Memorias I Congreso Latinoamericano de Sismología. II Congreso, Colombiano de Sismología,* Armenia (in Spanish).

Rhoades, D. A., A. Christophersen, S. Bourguignon, J. Ristau, and J. Salichon (2021). A depth dependent local magnitude scale for New Zealand earthquakes consistent with moment magnitude, *Bull. Seismol. Soc. Am.* **111,** 1056–1066, doi: 10.1785/0120200252.

Richter, C. F. (1935). An instrumental earthquake magnitude scale, *Bull. Seismol. Soc. Am.* **25,** no. 1, 1–32.

Rosencrantz, E., and P. Mann (1991). *Sea MARC II Mapping of Transform Faults in the Cayman Trough, 621. Caribbean Sea,* Geology, Geological Society of America, Boulder, Colorado, U.S.A., Vol. 19, 690–693.

Sandron, D., G. F. Gentile, S. Gentili, A. Sarao, A. Rebez, M. Santulin, and D. Slejko (2015). The Wood-Anderson of Trieste (northeast Italy): One of the last operating torsion seismometers, *Seismol. Res. Lett.* **86,** no. 6, 1645–1654, doi: 10.1785/0220150047.

Scordilis, E., D. Kementzetzidou, and B. Papazachos (2013). Local magnitude estimation in Greece, based on recordings of the Hellenic unified seismic network (HUSN), *Bull. Geol. Soc. Greece* **47,** 1241–1250.

Serrano, M., and L. Álvarez (1983). Desarrollo de la sismología instrumental en Cuba, *Investigaciones Sismológicas en Cuba,* 5–20, available at https://www.cenais.gob.cu/cenais (last accessed July 2023) (in Spanish).

Shumba, B. T., V. Midzi, B. Manzunzu, and J. R. Maritinkole (2023). Calibration of the local magnitude scale (M_l) for central southern Africa, *J. Seismol.* **27,** 291–304, doi: 10.1007/s10950-023-10139-7.

Uhrhammer, R. A., and E. R. Collins (1990). Synthesis of Wood–Anderson seismograms from broadband digital records, *Bull. Seismol. Soc. Am.* **80,** 702–716.

Vishwa, J., S. Chopra, and S. Kumar (2020). A local magnitude scale ML for the Saurashtra horst. An active intraplate region, Gujarat, India, *J. Earth Syst. Sci.* **129,** 114, doi: 10.1007/s12040-020-1379-z.

Wessel, P., and W. Smith (1991). Free software helps map and display data, *Eos Trans. AGU* **72,** 441–461.

Wessel, P., W. H. F. Smith, R. Scharroo, J. F. Luis, and F. Wobbe (2013). Generic mapping tools: Improved version released, *Eos Trans. AGU* **94,** 409–410, doi: 10.1002/2013EO450001.
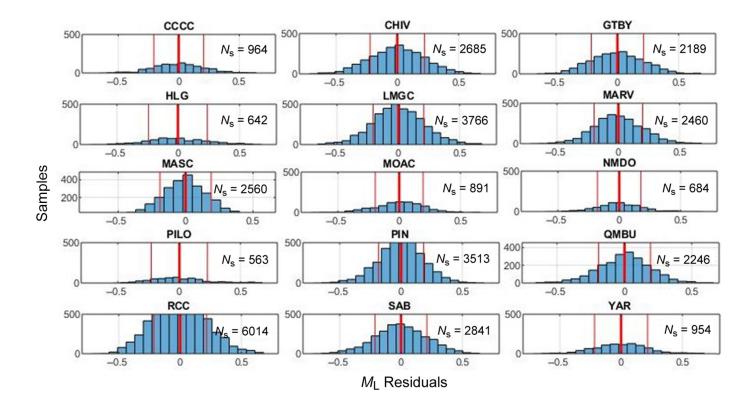
Appendix

We have selected from the earthquake catalog of the National Seismological Center of Cuba—a selection that includes earthquakes from 2011 to 2021 with magnitudes greater than

Figure A1. Seismicity in Cuba and surrounding areas from 2011 to 2021, taken from the CENAIS historical general catalog and reprocessed for this study by authors. The magnitude ranges from 0.1 to 7 is considered (no differentiation by magnitudes). The red triangles represent the broadband stations, and the inverted blue triangles show the short-period stations of the Cuban network. The Oriente fault is explicitly shown (black line). The color version of this figure is available only in the electronic edition.

Figure A2. Residuals distribution per station (number of samples versus residual values). The color version of this figure is available only in the electronic edition.

0.1° and up to 7°, recorded by the Cuban SSN during these years. Figure A1 shows the map of the local and regional earthquake epicenters for the whole geographic area covered by CENAIS seismic stations.

Figure A2 shows the number of samples and corresponding residuals for each seismological station.

The 2011–2021 Cuban earthquake catalog is provided as the supplemental material as data set DS01.